MATERIALS SCIENCE / **МАТЕРИАЛОВЕДЕНИЕ**

UDC 621:538.911:538.951
DOI 10.17073/0368-0797-2024-6-686-695

Original article
Оригинальная статья

Structural-phase state and properties of 56GM/(W + WC(Ni)) composite alloy obtained by wire electron beam additive manufacturing

A. V. Nikonenko ✉, **A. V. Vorontsov, N. N. Shamarin, V. R. Utyaganova, N. L. Savchenko, A. P. Zykova**

Institute of Strength Physics and Materials Science, Siberian Branch of the Russian Academy of Sciences (2/4 Akademicheskii Ave., Tomsk 634055, Russian Federation)

✉ aliska-nik@mail.ru

Abstract. The authors investigated the microstructure and mechanical characteristics of 56GM steel-based composite produced by wire electron-beam additive manufacturing with the addition of W + WC(Ni) powders during printing. The analysis demonstrates that 56GM/(W + WC(Ni)) composite alloy is characterised by a gradient structure consisting of 56GM base layer, 56GM – 56GM/(W + WC(Ni)) intermediate layer and 56GM/(W + WC(Ni)) composite layer. The base layer of 56GM steel is characterized by a multidirectional acicular structure, which corresponds to the ferrite-martensite state. In 56GM – 56GM/(W + WC(Ni)) intermediate layer the acicular structure becomes less pronounced. In 56GM/(W + WC(Ni)) composite layer an equiaxed grain structure is formed, with an average grain size of 8.59 μm, along the boundaries of which cracks are observed. WC particles are located mainly along the boundaries of small grains and in small quantities inside the grains themselves. It was found that 56GM/(W + WC(Ni)) composite is mainly composed of α-Fe (~80.6 vol. %), Ni (~6 vol. %), WC carbide phase (~10.3 vol. %) and γ-Fe (3 vol. %). The structure and properties of initial 56GM steel change both in the area of direct addition of alloying powder and in the underlying layers due to diffusion processes and infiltration of W + WC(Ni). Microhardness values increase from ~3.5 GPa to ~6.5 GPa with distance from the substrate to the composite layer. In uniaxial tensile tests, the ultimate tensile strength and yield strength values reached 1100 – 1200 MPa and 835 MPa in the intermediate layer, respectively.

Keywords: electron beam additive manufacturing, composite, 56GM steel, powder, WC(Ni) powder, structure, mechanical properties

Acknowledgements: The work was carried out within the framework of the state assignment of the Institute of Problems of Socio-Mechanical Problems of the Siberian Branch of the Russian Academy of Sciences, topic No. FWRW-2024-0001. The research was carried out using the equipment of the Nanotech Center of Collective Use of the Institute of Problems of Socio-Mechanical Problems of the Siberian Branch of the Russian Academy of Sciences.

For citation: Nikonenko A.V., Vorontsov A.V., Shamarin N.N., Utyaganova V.R., Savchenko N.L., Zykova A.P. Structural-phase state and properties of 56GM/(W + WC(Ni)) composite alloy obtained by wire electron beam additive manufacturing. *Izvestiya. Ferrous Metallurgy*. 2024;67(6):686–695. https://doi.org/10.17073/0368-0797-2024-6-686-695

Структурно-фазовое состояние и свойства композитного сплава 56GM/(W + WC(Ni)), полученного методом проволочного электронно-лучевого аддитивного производства

А. В. Никоненко, А. В. Воронцов, Н. Н. Шамарин, В. Р. Утяганова, Н. Л. Савченко, А. П. Зыкова

Институт физики прочности и материаловедения Сибирского отделения РАН (Россия, 634055, Томск, пр. Академический, 2/4)

aliska-nik@mail.ru

Аннотация. В работе исследовали микроструктуру и механические характеристики композита на основе стали 56GM, полученного методом проволочного электронно-лучевого аддитивного производства с введением при печати порошков W + WC(Ni). Показано, что композитный сплав 56GM/(W + WC(Ni)) характеризуется градиентной структурой, состоящей из основного слоя стали 56GM, промежуточного слоя 56GM – 56GM/(W + WC(Ni)) и композиционного слоя 56GM/(W + WC(Ni)). Основой слой 56GM характеризуется разнонаправленной игольчатой структурой, что соответствует феррито-мартенситному состоянию. В промежуточном слое 56GM – 56GM/(W + WC(Ni)) игольчатая структура становится менее выраженной. В композиционном слое 56GM/(W + WC(Ni)) формируется равноосная зеренная структура со средним размером зерен 8,59 мкм, по границам которых наблюдаются трещины. Частицы карбида вольфрама WC располагаются преимущественно по границам мелких зерен и в небольшом количестве внутри самих зерен. Методом рентгенофазового анализа установлено, что композит 56GM/(W + WC(Ni)) преимущественно состоит из α-Fe (~80,6 об. %), Ni (~6 об. %), карбидной фазы WC (~10,3 об. %) и незначительной доли γ-Fe (3 об. %). Структура и свойства исходной стали 56GM изменяются не только в области непосредственного добавления легирующего порошка, но и в нижележащих слоях из-за диффузионных процессов и инфильтрации порошка W + WC(Ni) при печати. Значения микротвердости по мере удаления от подложки до композиционного слоя увеличиваются примерно от 3,5 до 6,5 ГПа. Испытания на одноосное растяжение показали максимальные предел прочности и предел текучести в промежуточном слое, которые составили 1100 – 1200 и 835 МПа соответственно.

Ключевые слова: электронно-лучевое аддитивное производство, композит, сталь 56GM, порошок вольфрама, порошок WC(Ni), структура, механические свойства

Благодарности: Работа выполнена в рамках государственного задания Института физики прочности и материаловедения Сибирского отделения РАН, тема номер FWRW-2024-0001. Исследования выполнены с использованием оборудования ЦКП «Нанотех» Института физики прочности и материаловедения Сибирского отделения РАН.

Для цитирования: Никоненко А.В., Воронцов А.В., Шамарин Н.Н., Утяганова В.Р., Савченко Н.Л., Зыкова А.П. Структурно-фазовое состояние и свойства композитного сплава 56GM/(W + WC(Ni)), полученного методом проволочного электронно-лучевого аддитивного производства. *Известия вузов. Черная металлургия*. 2024;67(6):686–695. https://doi.org/10.17073/0368-0797-2024-6-686-695

Introduction

The incorporation of reinforcing materials (such as oxides, intermetallic compounds, nitrides, carbides, and borides) into a steel matrix enables the production of materials with enhanced performance characteristics due to the synergistic properties of the reinforcement and the matrix. These materials are known as metal-matrix composites (MMCs) [1]. The synthesis of MMCs is a highly effective approach to improving the mechanical properties of steel, including hardness, strength, fatigue life, and wear resistance [2].

Traditionally, MMCs are produced using casting or powder metallurgy methods. These techniques are time-consuming and challenging to control. Furthermore, the high cost of casting molds, coarse-grained microstructures, and limitations associated with the formation of undesirable interfacial compounds between the reinforcing particles and the matrix present significant challenges in the fabrication of MMCs [3].

Hybrid electron beam additive manufacturing technology, which involves the simultaneous or programmed feeding of wire and powder filaments, is an advanced additive manufacturing approach that enables the production of metallic components and composites with tailored microstructures. Recently, this technology has been the subject of intensive research and holds significant potential for creating novel metallic materials with unique properties [4 – 6].

Tungsten carbide (WC) is well-suited as a reinforcing particle for iron-based alloys due to its high melting point, thermal stability, strength, hardness, good wettability, and a coefficient of thermal expansion similar to that of iron. Consequently, there have been substantial efforts in recent years to fabricate WC/Fe composites using various methods, including additive manufacturing [7]. Particular attention has been paid to improving the microhardness and wear resistance of such composites, which result from the strong adhesion of tungsten carbide particles to the iron-based matrix via a reaction

layer. However, the development of high-performance MMCs has revealed challenges, such as the formation of thick, brittle reaction layers between the reinforcing particles and the matrix, driven by the formation of carbides like Me_3C [8]. These reaction layers frequently lead to cracks that propagate along the tungsten carbide/matrix interface [9]. As a result, the tungsten carbide particles lose their ability to effectively bear the load, compromising the mechanical properties of the composite material. Controlling the phase evolution at the interface between tungsten carbide reinforcing particles and the iron-based matrix must consider the diffusion of tungsten, carbon, iron, and other alloying elements, which is particularly challenging due to the non-equilibrium conditions of additive manufacturing associated with high energy input. Careful control of the reaction layer thickness is essential to ensure the load-bearing capacity of the tungsten carbide particles [10]. Furthermore, it is crucial to investigate how tungsten and carbon influence phase transformations in the iron-based matrix during rapid solidification in additive manufacturing, as they significantly expand the stability ranges of ferritic and austenitic phases, respectively [11].

It is well established that the nickel-tungsten carbide (Ni – WC) system exhibits superior properties when used for producing highly wear-resistant overlay deposits on various tools employed in the oil and gas industry [12]. In the Ni – WC system, tungsten carbide particles provide the desired wear resistance, while nickel alloys contribute relatively high impact toughness, mitigating the embrittlement of tungsten carbides [13].

It is also known that tungsten additions slow down the kinetics of carbide precipitation from steel alloying elements due to its low diffusion rate [14; 15]. In [16], the authors reported that introducing tungsten into hot-work tool steel alloyed with Cr – Mo – V improves mechanical properties during high-temperature tempering and increases resistance to softening by suppressing the coarsening of nanoscale carbides. Similarly, [17] demonstrated that adding tungsten to Cr – Mo alloyed steel enhances high-temperature strength by inhibiting dislocation recovery during tempering above 650 °C, resulting in a reduction in the size of $Me_{23}C_6$ carbides.

Recently, there has been a growing demand for materials capable of withstanding complex stresses, including thermal, mechanical, chemical, electromagnetic, and, potentially, neutron irradiation [18; 19]. The ability to function under such extreme conditions poses significant challenges in material development, often requiring combinations of multiple materials. When two or more materials are used, several challenges arise in integrating them into a compact composite. These include mismatched thermal and mechanical properties leading to stress concentration at the interface, physicochemical incompatibility, insufficient wettability or high mutual reactivity, and neutron-physical issues with some solders, among others [20 – 22].

The objective of this study is to investigate the microstructure and mechanical properties of steel matrix composites based on heat-resistant, highly alloyed steel with two types of reinforcing particles: tungsten particles and nickel-coated tungsten carbide particles. This composite was synthesized using a hybrid wire-and-powder electron beam additive manufacturing method.

Materials and methods

To produce the 56GM/(W + WC(Ni)) composite, 56GM steel wire (equivalent to 40Kh9S2 steel) with a diameter of 1 mm and the following chemical composition (wt. %) was used: Fe 86.9; Cr 9.24; Si 3.02; C 0.44; Mn 0.4.

Reinforcing powders of tungsten and nickel-coated tungsten carbide (WC(Ni)) were used in a mass ratio of 1:1. SEM images of tungsten powder particles and WC(Ni) particles are shown in Fig. 1, *a* and *c*. According to *X*-ray phase analysis, the tungsten powder particles contain a minor fraction of WO_3 oxide (Fig. 1, *b*). The *X*-ray phase analysis of WC(Ni) powder identified the presence of tungsten carbide (WC) and nickel phases (Fig. 1, *d*).

The 56GM/(W + WC(Ni)) composite was fabricated as follows. Using wire electron beam additive manufacturing (EBAM), layers of 56GM steel were deposited on a 12Kh18N10 stainless steel substrate (Fig. 2, *a*). After depositing nine layers of 56GM, 0.3 g of W + WC(Ni) powder was introduced onto the workpiece using a powder feeder (Fig. 2, *b*). A layer of 56GM wire was then deposited, which partially melted the W + WC(Ni) powders and the underlying 56GM layer (Fig. 2, *c*). Subsequently, another 0.3 g layer of W + WC(Ni) powder was applied using the powder feeder, followed by another layer of 56GM wire. This process was repeated three times, resulting in three layers of W + WC(Ni) powder alternated with layers of 56GM steel (each layer being 1 mm thick) (Fig. 2, *d*). The final samples measured 72×36×9 mm.

To study the structural-phase composition and mechanical properties of the 56GM/(W + WC(Ni)) composite, samples were extracted from three zones: the matrix, the intermediate layer, and the upper composite layer. The samples were prepared following standard procedures, which included grinding with sandpaper and polishing with diamond pastes (grit sizes 14/10, 3/2, and 1/0). To reveal microstructural elements, the polished sample surfaces were chemically etched using a reagent composed of $CuSO_4$ (0.008 kg) + H_2O (0.04 L) + HCl (0.04 L).

The macro- and microstructure of the samples were examined using an Altami Met 1S optical microscope, an Olympus confocal laser microscope, and scanning electron microscopy (SEM) (Thermo Fisher Scientific Apreo S LoVac equipped with an energydispersive spect-

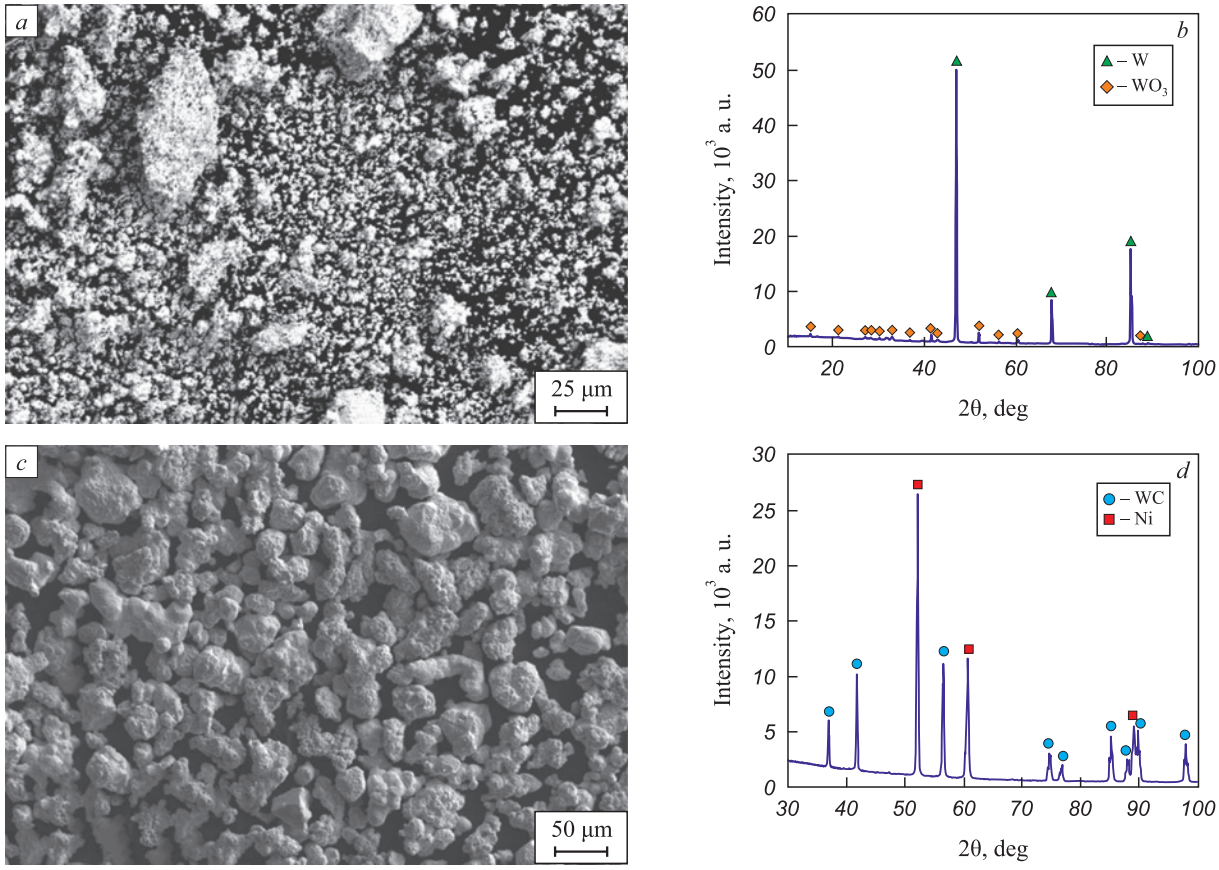

Fig. 1. SEM images (*a*, *c*) and *X*-ray diffraction patterns (*b*, *d*) of the initial W powder (*a*, *b*) and WC(Ni) powder (*c*, *d*)

Рис. 1. РЭМ-изображения (*a*, *c*) и рентгенограммы (*b*, *d*) исходного порошка вольфрама (*a*, *b*) и порошка карбида вольфрама WC(Ni) (*c*, *d*)

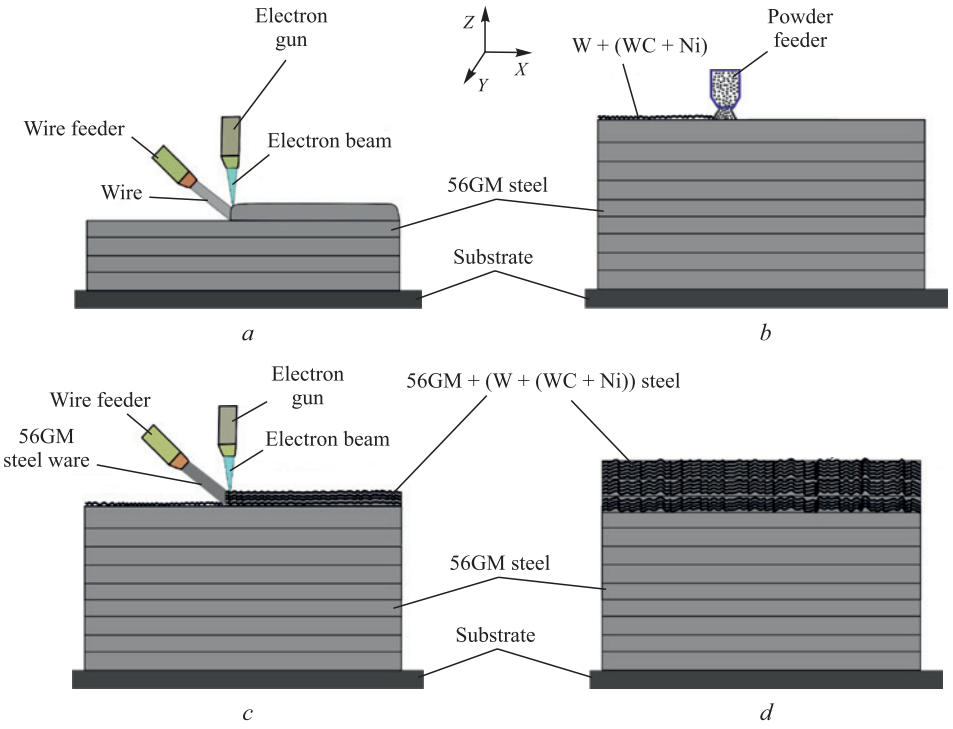

Fig. 2. Scheme of deposition of layers of the composite sample 56GM/(W + (WC(Ni))

Рис. 2. Схема нанесения слоев композиционного образца 56GM/(W + (WC(Ni))

rometer (EDS)). Particle sizes were measured using the secant method on prepared metallographic sections. *X*-ray phase analysis (XRD) was performed on a DRON-7 *X*-ray diffractometer (CoK_α radiation).

Microhardness was measured using a TBM 5215 A Tochline hardness tester with a 0.5 N load and a dwell time of 10 s. Uniaxial tensile tests were conducted on a UTS-110M-100 universal testing machine at room temperature with a crosshead speed of 1 mm/min. For tensile testing, flat specimens were cut along and across the printing direction, shaped as proportionally reduced blades according to GOST 1497, with working section dimensions of 12×2.7×1.5 mm. The specimens were extracted from characteristic regions of the composite material (matrix, intermediate layer, and upper composite layer).

Results and discussion

Fig. 3, *a* shows an optical image of the 56GM/(W + + WC(Ni)) composite alloy in the *ZOY* section, where several characteristic zones can be distinguished: *1* – stainless steel substrate (not considered in this study); *2* – layer of 56GM steel; *3* – intermediate layer 56GM – 56GM/(W + WC(Ni)); *4* – composite layer (W + WC(Ni))/56GM. In the *ZOY* cross-section of the 56GM/(W + WC(Ni)) sample (layer *2*), a significant number of melt pool boundaries, formed during the printing of 56GM steel layers, are observed. Layer *3*, the intermediate layer, features a distinct boundary between the printed matrix and the composite layers (Fig. 3, *a*). According to the results of *X*-ray tomography of the 56GM/(W + WC(Ni)) sample (Fig. 3, *b*), no macroscopic defects such as pores or cracks were detected in any of the analyzed zones (*1* – *3*) shown in Fig. 3, *a*.

X-ray phase analysis revealed that the 56GM/(W + WC(Ni)) composite primarily consists of α-Fe (~83.69 vol. %), Ni (~6 vol. %), and the WC carbide phase (~10.31 vol. %) (Fig. 3, *c*). Additionally, a small fraction of γ-Fe was observed in the composite layer, whereas no traces of γ-Fe were detected in the base alloy or the intermediate layer.

According to SEM analysis, the 56GM steel (layer *2*) exhibits a multidi-rectional acicular structure corresponding to a ferrite-martensite state (indicated by the red arrow, Fig. 4, *a*). The matrix of the composite alloy primarily consists of ~78 at. % Fe, ~12 at. % Cr, and ~6 at. % Si, which matches the initial steel composition (spectrum *3*, Fig. 4, *a*, *b*). The concentrations of tungsten and nickel in the base 56GM alloy are low, approximately 2 at. % each. Along the grain boundaries of the base layer of 56GM steel, fine particles are observed, which may result from infiltration along the grain boundaries or microcracks, as well as diffusion during composite printing (Fig. 4, *a*). EDS analysis of these particles shows ~66 at. % Fe, ~18 at. % Cr, ~7 at. % W, ~4 at. % Ni, and ~5 at. % Si (spectra *1* – *2*, Fig. 4, *a*, *b*). Since the EDS analysis captures a larger area, including both the particle and the matrix, it can be inferred based on XRD data that these particles are tungsten carbide (WC).

In the intermediate layer 56GM – 56GM/(W + WC(Ni)) (layer *3*, Fig. 3, *a*), the acicular structure becomes less pronounced (Fig. 4, *c*). However, the elemental composition of the grains in the transition zone is comparable

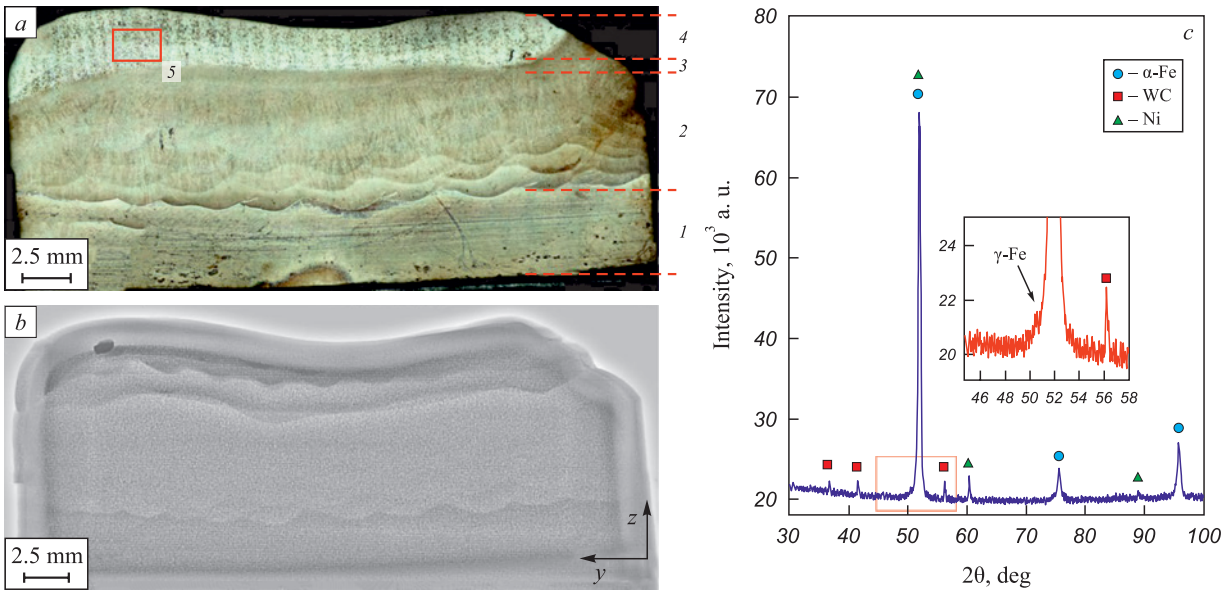

Fig. 3. Macrostructure (*a*), fluoroscopy (*b*) and *X*-ray pattern (*c*) of 56GM/(W + WC(Ni)) composite:
1 – substrate; *2* – layer of 56GM steel; *3* – intermediate layer; *4* – 56GM/(W + WC(Ni))composite layer; *5* – sample for XRD

Рис. 3. Макроструктура (*a*), рентгеноскопия (*b*) и рентгенограмма (*c*) композита 56GM/(W + WC(Ni)):
1 – подложка; *2* – слой стали 56GM; *3* – промежуточный слой; *4* – композиционный слой 56GM/(W + WC(Ni)); *5* – образец для РФА

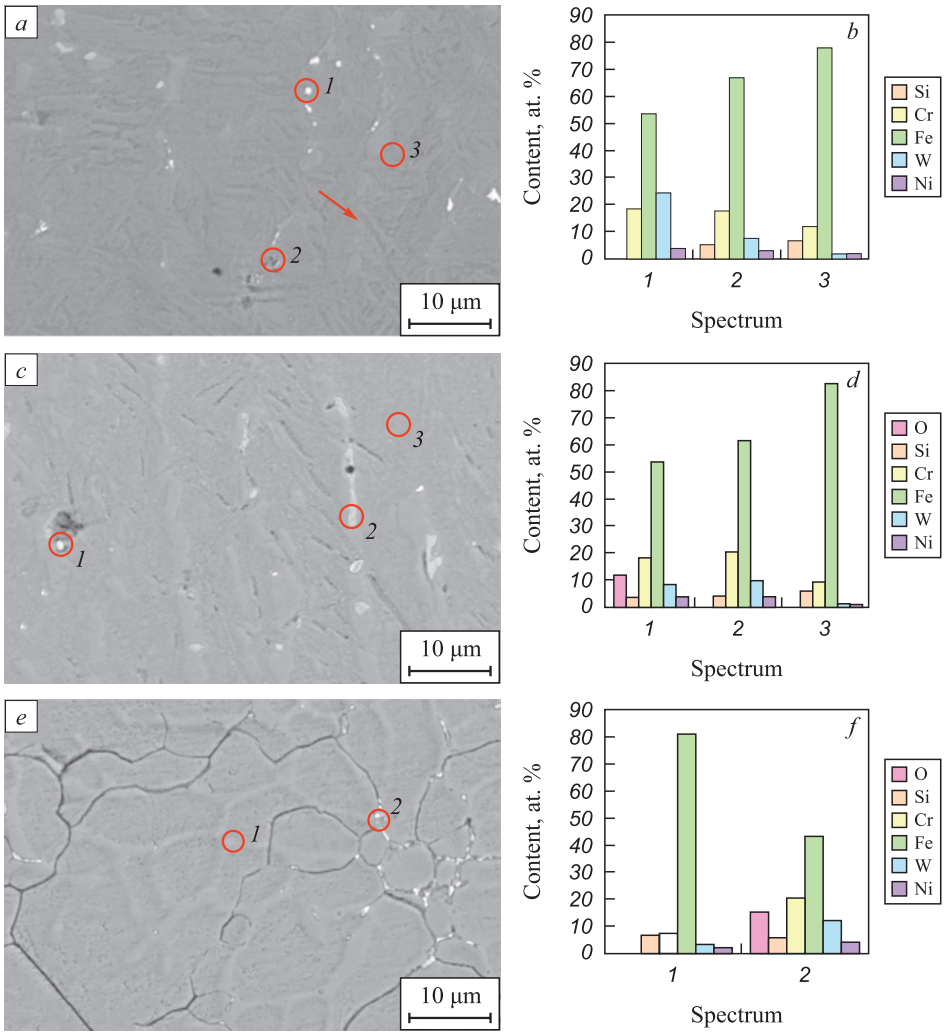

Fig. 4. SEM images and elemental composition of 56GM/(W + WC(Ni)) composite sample:
a, *b* – layer of 56GM steel (layer *2*); *c*, *d* – intermediate layer (layer *3*); *e*, *f* – 56GM/(W + WC(Ni)) composite layer

Рис. 4. РЭМ-изображения и элементный состав композиционного образца 56GM/(W + WC(Ni));
a, *b* – сталь 56GM (слой *2*); *c*, *d* – промежуточный слой (слой *3*); *e*, *f* – композиционный слой 56GM/(W + WC(Ni))

to that of the base layer of 56GM steel (spectrum *3*, Fig. 4, *c*, *d*). Similar to the base alloy, fine tungsten carbide (WC) particles are observed along the grain boundaries in the intermediate layer, with an average size of 2.64 μm (spectra *1* – *2*, Fig. 4, *c*, *d*).

In the composite layer 56GM/(W + WC(Ni)) (layer *4*, Fig. 3, *a*), an equiaxed grain structure is formed, with an average grain size of 8.59 μm. Cracks are observed along the grain boundaries (Fig. 4, *e*). EDS analysis of these grains also corresponds to the elemental composition of the base layer (spectrum *1*, Fig. 4, *e*, *f*): ~81 at. % Fe, ~7 at. % Cr, and ~7 at. % Si. WC powder particles are predominantly located within the cracks (along the boundaries of small grains) and, to a lesser extent, inside the grains (spectrum *2*, Fig. 4, *e*, *f*). The volume fraction of WC particles in the composite layer significantly increases compared to their fraction in the base alloy and the intermediate layer. According to XRD data, in addition to the main phases α-Fe (~80.6 vol. %), Ni (~6 vol. %), and WC (~10.3 vol. %), a minor fraction of γ-Fe (~3 vol. %) is present in the composite layer (Fig. 3, *c*).

Microhardness measurements were conducted on the cross-section *ZOY* of the 56GM/(W + WC(Ni)) composite in two regions (Fig. 5, *a*). In all cases, microhardness increased when measured in the direction from the substrate to the composite layer (Fig. 5, *a*). The microhardness values for the base intermediate and composite layers were approximately 3.5, 6.1, and 6.5 GPa, respectively.

Tensile tests on samples extracted from the base alloy and intermediate layer in the *ZOY* and *ZOX* cross-sections demonstrated ductile fracture behavior (samples 1.1, 2.1, 2.2, Fig. 5, *b* – *d*). For samples from the region of the base layer of 56GM steel, the ultimate tensile strength and yield strength were approximately 1000 and 650 MPa, respec-

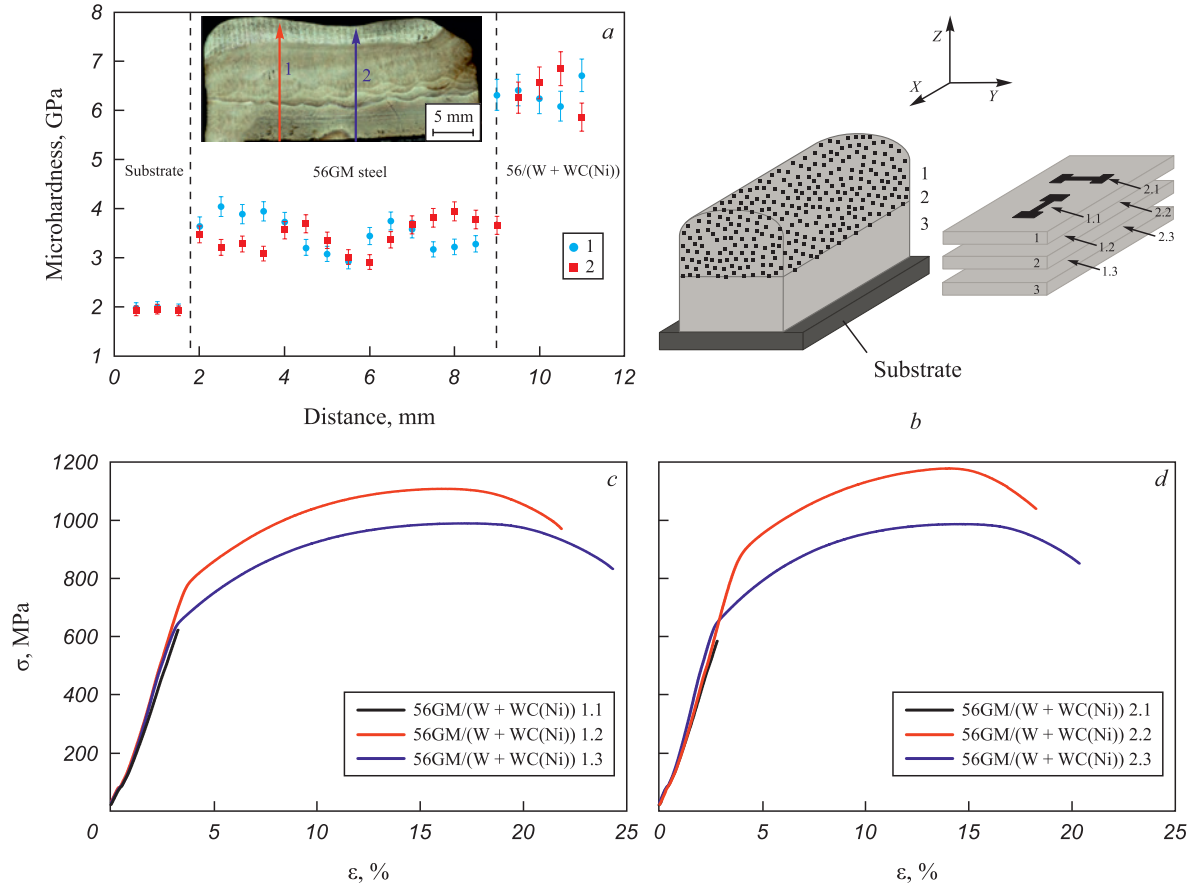

Fig. 5. Microhardness values (*a*), sample cutting diagram for tensile test (*b*), tensile values according to the sample cutting diagram (*c*, *d*)

Рис. 5. Значения микротвердости (*a*), схема вырезки образцов для испытания на растяжение (*b*), значения растяжения согласно схеме вырезки образцов (*c*, *d*)

tively (Fig. 5, *c*, *d*). For samples from the intermediate region (56GM – 56GM/(W + WC(Ni))), the ultimate tensile strength and yield strength reached 1100 – 1200 MPa and ~835 MPa, respectively – representing increases of 10 and 28 % compared to the base alloy (Fig. 5, *c*, *d*). For samples extracted from the composite layer region in the *ZOY* and *ZOX* cross-sections, the ultimate tensile strength values were 590 and 620 MPa, respectively, and the yield strength was ~570 MPa (samples 1.3, 3.1, Fig. 5, *b* – *d*). Due to the high volume fraction of brittle carbide particles located at the grain boundaries of 56GM steel, the relative elongation decreases to 3 %. A composite layer containing approximately 10 vol. % tungsten carbide is considered typical for metal-matrix composites, for which mechanical properties are traditionally assessed using compression rather than tensile testing [11].

It is well known that during additive manufacturing, significant diffusion of carbon from tungsten carbide (WC) particles into the α-Fe-based matrix occurs due to the formation of the melt pool. This diffusion significantly influences the phase formation of the matrix near the reinforcing carbide particles, as carbon is an austenite-promoting element. A substantial amount of diffused carbon likely integrates into the α-Fe matrix as interstitial atoms, driving the phase transformation from α-Fe to γ-Fe in the composite layer (Fig. 3, *c*). Furthermore, the nickel coating on the tungsten carbide particles is also an austenite-promoting element. For instance, additional nickel alloying in high-chromium steels can produce fully austenitic structures at room temperature under specific chromium-to-nickel ratios.

Numerous studies have reported that ferrite-martensite microstructures typically revert to austenite during the melting of the subsequent powder layer, as the temperature in some regions of the melt pool exceeds the austenite transformation finish temperature due to the constant heat flow from the molten zones to the substrate [23]. It is expected that the austenite would subsequently transform into martensite due to the high intrinsic cooling rate. As noted earlier, neither the base alloy nor the intermediate layer exhibited traces of γ-Fe, and their phase composition consisted entirely of α-Fe. However, in the composite layer, a small fraction of austenite did not transform into α-Fe during cooling due to the presence of tungsten carbide and nickel particles (Fig. 3, *c*).

The absence of interaction between iron and tungsten carbide (WC) form-ing carbides such as Me_3C, as

observed in this study, can be attributed to the beneficial effect of tungsten. Tungsten's slow diffusion rate reduced the kinetics of such carbide formation [14; 15].

Conclusions

The microstructure and mechanical properties of a composite alloy based on 56GM steel, produced using wire electron beam additive manufacturing with the incorporation of W + WC(Ni) powders during printing, were investigated. The 56GM/(W + WC(Ni)) composite alloy features a gradient structure consisting of the base layer of 56GM steel, an intermediate layer (56GM – 56GM/(W + WC(Ni))), and a composite layer (56GM/(W + WC(Ni))). The base layer of 56GM steel is composed of ferrite-martensite grains with isolated tungsten carbide (WC) particles located along the grain boundaries. The ultimate tensile strength and yield strength in the base metal zone were approximately 1000 and 650 MPa, respectively. In the composite layer, an equiaxed ferrite-martensite grain structure with a small fraction of austenite forms. was observed. Cracks were found along the grain boundaries, where tungsten carbide (WC) particles were concentrated. The volume fraction of WC particles in the composite layer was significantly higher than in the base layer of 56GM steel, resulting in a 40 % reduction in tensile strength and brittle fracture. Nonetheless, microhardness increased steadily from the substrate to the composite layer, ranging from 3.5 to 6.5 GPa.

The introduction of nickel-coated tungsten carbide (WC) particles shows considerable potential for fine-tuning the strength and ductility of steel materials by adjusting the volume fractions of austenitic and ferritic phases.

The results suggest that incorporating W + WC(Ni) powders into the surface layers of 56GM steel using electron beam additive manufacturing can enhance the tribological properties of the resulting composite material. This method holds significant promise for producing iron-based components with outstanding performance characteristics.

References / Список литературы

1. Tjong S.C. Recent progress in the development and properties of novel metal matrix nanocomposites reinforced with carbon nanotubes and graphene nanosheets. *Materials Science and Engineering: R: Reports*. 2013;74(10):281–350. https://doi.org/10.1016/j.mser.2013.08.001
2. Radhamani A.V., Lau H.C., Ramakrishna S. CNT-reinforced metal and steel nanocomposites: A comprehensive assessment of progress and future directions. *Composites Part A: Applied Science and Manufacturing*. 2018;114:170–187. https://doi.org/10.1016/j.compositesa.2018.08.010
3. AlMangour B., Grzesiak D., Yang J.-M. Selective laser melting of TiC reinforced 316L stainless steel matrix nanocomposites: Influence of starting TiC particle size and volume content. *Materials & Design*. 2016;104:141–151. https://doi.org/10.1016/j.matdes.2016.05.018
4. Filippov A.V., Khoroshko E.S., Shamarin N.N., Savchenko N.L., Moskvichev E.N., Utyaganova V.R., Kolubaev E.A., Smolin A.Yu., Tarasov S.Yu. Characterization of gradient CuAl–B_4C composites additively manufactured using a combination of wire-feed and powder-bed electron beam deposition methods. *Journal of Alloys and Compounds*. 2021;859:157824. https://doi.org/10.1016/j.jallcom.2020.157824
5. Zykova A., Chumaevskii A.V, Vorontsov A., Shamarin N., Panfilov A., Knyazhev E., Moskvichev E., Gurianov D., Savchenko N., Kolubaev E., Tarasov S. Microstructural evolution of AA5154 layers intermixed with Mo powder during electron beam wire-feed additive manufacturing (EBAM). *Metals*. 2022;12(1):109. https://doi.org/10.3390/met12010109
6. Utyaganova V.R., Chumaevskii A.V., Shamarin N.N., Moskvichev E.N., Vorontsov A.V., Gurianov D.A., Knyazhev E.O., Savchenko N.L. Regularities of structure formation and properties of composite materials based on aluminum–manganese bronze produced by electron beam additive manufacturing with the addition of iron, nickel, and tungsten powders during printing. *Russian Physics Journal*. 2023;65(9):1584–1591. https://doi.org/10.1007/s11182-023-02805-7
7. Yan X.C., Chen C.Y., Zhao R.X., Ma W.Y., Bolot R., Wang J., Ren Z.M., Liao H.L., Liu M. Selective laser melting of WC reinforced maraging steel 300: Microstructure characterization and tribological performance. *Surface and Coatings Technology*. 2019;371:355–365. https://doi.org/10.1016/j.surfcoat.2018.11.033
8. Gu D.D., Ma J., Chen H., Lin K., Xi L. Laser additive manufactured WC reinforced Fe-based composites with gradient reinforcement/matrix interface and enhanced performance. *Composite Structures*. 2018;192:387–396. https://doi.org/10.1016/j.compstruct.2018.03.008
9. Wang J.D., Li L.Q., Tao W. Crack initiation and propagation behavior of WC particles reinforced Fe-based metal matrix composite produced by laser melting deposition. *Optics and Laser Technology*. 2016;82:170–182. https://doi.org/10.1016/j.optlastec.2016.03.008
10. Kang N., Ma W., Heraud L., El Mansori M., Li F., Liu M., Liao H. Selective laser melting of tungsten carbide reinforced maraging steel composite. *Additive Manufacturing*. 2018;22:104–110. https://doi.org/10.1016/j.addma.2018.04.031
11. Chen H., Gu D., Kosiba K., Lu T., Deng L., Xi L., Kühn U. Achieving high strength and high ductility in WC-reinforced iron-based composites by laser additive manufacturing. *Additive Manufacturing*. 2020;35:101195. https://doi.org/10.1016/j.addma.2020.101195
12. Farahmand P., Kovacevic R. Corrosion and wear behavior of laser cladded Ni–WC coatings. *Surface and Coatings Technology*. 2015;276:121–135. https://doi.org/10.1016/j.surfcoat.2015.06.039
13. Liu W., Gao D. Microstructure and wear of Ni-WC hardfacing used for steel-body PDC bits. *International Journal of Refractory Metals and Hard Materials*. 2021;101:105683. https://doi.org/10.1016/j.ijrmhm.2021.105683
14. Ding H., Yuan Z., Liu T., Chen L., Zhou Y., Cao Y., Cao F., Luo R., Cheng X. Microstructure and high-temperature tensile behavior of modified H13 steel with the addition of tung-

sten, molybdenum, and lowering of chromium. *Materials Science and Engineering: A*. 2023;866:144655. https://doi.org/10.1016/j.msea.2023.144655

15. Won Y.-J., Kwon Y.-J., You J.-S., Park S.-S., Cho K.-S. Role of W addition in reducing heat checking and enhancing the mechanical properties of hot work tool steel. *Journal of Materials Research and Technology*. 2023;24:3413–3422. https://doi.org/10.1016/j.jmrt.2023.04.008
16. Xiang S., Wu R., Li W., Hu T., Huang S. Improved red hardness and toughness of hot work die steel through tungsten alloying. *Journal of Materials Engineering and Performance*. 2021;30(8):6146–6159. https://doi.org/10.1007/s11665-021-05793-2
17. Hong S.G., Lee W.B., Park C.G. The effects of tungsten addition on the microstructural stability of 9Cr–Mo Steels. *Journal of Nuclear Materials*. 2001;288(2-3):202–207. https://doi.org/10.1016/S0022-3115(00)00558-4
18. Matějíček J., Boldyryeva H., Brožek V., Sachr P., Chráska T., Pala Z. W–steel and W–WC–steel composites and FGMs produced by hot pressing. *Fusion Engineering and Design*. 2015;100:364–370. https://doi.org/10.1016/j.fusengdes.2015.06.154
19. Bolt H., Barabash V., Krauss W., Linke J., Neu R., Suzuki S., Yoshida N., Team A.U. Materials for the plasma-facing components of fusion reactors. *Journal of Nuclear Materials*. 2004;329-333(A):66–73. https://doi.org/10.1016/j.jnucmat.2004.04.005
20. Odegard B.C., Cadden C.H., Watson R.D., Slattery K.T. A review of the US joining technologies for plasma facing components in the ITER fusion reactor. *Journal of Nuclear Materials*. 1998;258-263(1):329–334. https://doi.org/10.1016/S0022-3115(98)00402-4
21. Merola M., Akiba M., Barabash V., Mazul I. Overview on fabrication and joining of plasma facing and high heat flux materials for ITER. *Journal of Nuclear Materials*. 2002; 307-311(2):1524–1532. https://doi.org/10.1016/S0022-3115(02)01070-X
22. Hamilton N.R., Wood J., Galloway A., Robbie M.B.O., Zhang Y. The metallurgy, mechanics, modelling and assessment of dissimilar material brazed joints. *Journal of Nuclear Materials*. 2013;432(1-3):42–51. https://doi.org/10.1016/j.jnucmat.2012.07.022
23. Holzweissig M.J., Taube A., Brenne F., Schaper M., Niendorf T. Microstructural characterization and mechanical performance of hot work tool steel processed by selective laser melting. *Metallurgical and Materials Transactions B*. 2015; 46:545–549. https://doi.org/10.1007/s11663-014-0267-9

Information about the Authors / Сведения об авторах

Alisa V. Nikonenko, *Cand. Sci. (Eng.), Junior Researcher of the Laboratory of Structural Design of Advanced Materials,* Institute of Strength Physics and Materials Science of Siberian Branch of Russian Academy of Sciences
ORCID: 0000-0003-0937-1329
E-mail: aliska-nik@mail.ru

Andrei V. Vorontsov, *Cand. Sci. (Eng.), Research Associate of the Laboratory of Structural Design of Advanced Materials,* Institute of Strength Physics and Materials Science of Siberian Branch of Russian Academy of Sciences
ORCID: 0000-0002-4334-7616
E-mail: vav@ispms.ru

Nikolai N. Shamarin, *Junior Researcher of the Laboratory of Local Metallurgy in Additive Technologies,* Institute of Strength Physics and Materials Science of Siberian Branch of Russian Academy of Sciences
ORCID: 0000-0002-4649-6465
E-mail: shnn@ispms.ru

Veronika R. Utyaganova, *Cand. Sci. (Eng.), Research Associate of the Laboratory Local Metallurgy in Additive Technologies,* Institute of Strength Physics and Materials Science of Siberian Branch of Russian Academy of Sciences
ORCID: 0000-0002-2303-8015
E-mail: veronika_ru@ispms.ru

Nickolai L. Savchenko, *Dr. Sci. (Eng.), Leading Researcher of the Laboratory for Quality Control of Materials and Structures,* Institute of Strength Physics and Materials Science of Siberian Branch of Russian Academy of Sciences
ORCID: 0000-0001-8254-5853
E-mail: savnik@ispms.ru

Anna P. Zykova, *Cand. Sci. (Phys.-Math.), Senior Researcher, Head of the Laboratory of Structural Design of Advanced Materials,* Institute of Strength Physics and Materials Science of Siberian Branch of Russian Academy of Sciences
ORCID: 0000-0001-8779-3784
E-mail: zykovaap@mail.ru

Алиса Владимировна Никоненко, *к.т.н., младший научный сотрудник лаборатории структурного дизайна перспективных материалов,* Институт физики прочности и материаловедения Сибирского отделения РАН
ORCID: 0000-0003-0937-1329
E-mail: aliska-nik@mail.ru

Андрей Владимирович Воронцов, *к.т.н., научный сотрудник лаборатории структурного дизайна перспективных материалов,* Институт физики прочности и материаловедения Сибирского отделения РАН
ORCID: 0000-0002-4334-7616
E-mail: vav@ispms.ru

Николай Николаевич Шамарин, *младший научный сотрудник лаборатории локальной металлургии в аддитивных технологиях,* Институт физики прочности и материаловедения Сибирского отделения РАН
ORCID: 0000-0002-4649-6465
E-mail: shnn@ispms.ru

Вероника Рифовна Утяганова, *к.т.н., научный сотрудник лаборатории локальной металлургии в аддитивных технологиях,* Институт физики прочности и материаловедения Сибирского отделения РАН
ORCID: 0000-0002-2303-8015
E-mail: veronika_ru@ispms.ru

Николай Леонидович Савченко, *д.т.н., ведущий научный сотрудник лаборатории контроля качества материалов и конструкций,* Институт физики прочности и материаловедения Сибирского отделения РАН
ORCID: 0000-0001-8254-5853
E-mail: savnik@ispms.ru

Анна Петровна Зыкова, *к.ф.-м.н., старший научный сотрудник, заведующий лабораторией структурного дизайна перспективных материалов,* Институт физики прочности и материаловедения Сибирского отделения РАН
ORCID: 0000-0001-8779-3784
E-mail: zykovaap@mail.ru

Contribution of the Authors / Вклад авторов

A. V. Nikonenko – performing microstructure studies by optical microscopy, formation of the main concept of the article, selection of illustrations, description of the results.
A. V. Vorontsov – analysis of *X*-ray diffraction data, performing mechanical tensile tests.
N. N. Shamarin – EBAM printing of samples, sample preparation.

V. R. Utyaganova – performing microstructure studies by scanning electron microscopy, description of the results.

N. L. Savchenko – *X*-ray analysis, processing and analysis of microstructural findings, editing the article final version.

A. P. Zykova – analysis of experimental data, revision of the text, formation of conclusions, editing of the final version of the article.

А. В. Никоненко – выполнение исследований микроструктуры методом оптической микроскопии, формирование основной концепции статьи, оформление иллюстраций, описание результатов.
А. В. Воронцов – анализ данных рентгеноструктурного анализа, проведение механических испытаний на растяжение.
Н. Н. Шамарин – печать образцов методом ЭЛАП, пробоподготовка образцов.
В. Р. Утяганова – выполнение исследований микроструктуры методом сканирующей электронной микроскопии; описание результатов.
Н. Л. Савченко – выполнение исследований методом рентгенофазового анализа, обработка и анализ результатов микроструктурных исследований, редактирование финальной версии статьи.
А. П. Зыкова – анализ экспериментальных данных, доработка текста, формирование выводов, редактирование финальной версии статьи.

Received 19.06.2024
Revised 21.08.2024
Accepted 17.10.2024

Поступила в редакцию 19.06.2024
После доработки 21.08.2024
Принята к публикации 17.10.2024